Ambipolar Insulator-to-Metal Transition in Black Phosphorus by Ionic-Liquid Gating

Yu Saito[*,†] **and Yoshihiro Iwasa**[†,‡]

[†]Quantum-Phase Electronics Center (QPEC) and Department of Applied Physics, The University of Tokyo, Tokyo 113-8656, Japan and [‡]RIKEN Center for Emergent Matter Science (CEMS), Wako 351-0198, Japan

ABSTRACT We report ambipolar transport properties in black phosphorus using an electric-double-layer transistor configuration. The transfer curve clearly exhibits ambipolar transistor behavior with an ON−OFF ratio of $\sim 5 \times 10^3$. The band gap was determined as $\cong$0.35 eV from the transfer curve, and Hall-effect measurements revealed that the hole mobility was $\sim$190 cm^2/(V s) at 170 K, which is 1 order of magnitude larger than the electron mobility. By inducing an ultrahigh carrier density of $\sim 10^{14}$ cm^{-2}, an electric-field-induced transition from the insulating state to the metallic state was realized, due to both electron and hole doping. Our results suggest that black phosphorus will be a good candidate for the fabrication of functional devices, such as lateral p−n junctions and tunnel diodes, due to the intrinsic narrow band gap.

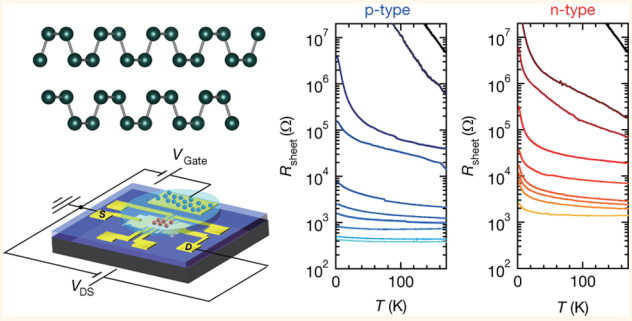

KEYWORDS: two-dimensional (2D) materials · ambipolar · black phosphorus · electric-double-layer transistor (EDLT) · insulator-to-metal transition · capacitance · localization

Since the discovery of graphene,[1−3] various two-dimensional (2D) materials,[4] including transition metal dichalcogenides (TMDCs), have been extensively investigated due to their promising electronic properties and potential applications. Despite the extremely high mobility in graphene, the absence of a band gap hinders the achievement of a high ON−OFF ratio. This has led to intensive research in other 2D materials that have an intrinsic band gap.[4] Among them, TMDCs, such as MoS_2 and WSe_2, which have finite band gaps, not only have enabled the fabrication of high-performance field effect transistor (FET) devices[5] but have also paved the way for the realization of novel optoelectronic and valleytronic devices.[6,7]

Recently, a new elemental 2D layered material, the black phosphorus (BP) monolayer, as well as its multilayers and field effect devices, has been fabricated by mechanical exfoliation.[8−11] BP is a van der Waals type semiconducting layered material with a puckered honeycomb structure, where each phosphorus atom is covalently bonded with three adjacent phosphorus atoms[12−14] (Figure 1a) and has a direct band gap of 0.3 eV (bulk) to 2 eV (monolayer), depending on the number of layers.[8] This tunable band gap may be useful for photodetectors and other optoelectronics devices. Moreover, in addition to the bulk properties of BP, including pressure-induced semiconductor to metal[15,16] and superconductor transitions,[17,18] the FET of the multilayer forms has been reported by several groups to exhibit p-type operation,[8−11] with a mobility of 200−300 cm^2/(V s) at room temperature.

The dominant p-type FET action, as compared with the n-type, is due to unintentionally doped hole carriers in BP multilayers. However, a band structure calculation[8] has indicated that the effective masses of the conduction and the valence band do not differ very much, and a comparable FET operation might thus be possible. Examination of the electron and hole transport in a single FET configuration is crucial for understanding the carrier accumulation and transport mechanisms, as well as for fabricating

* Address correspondence to saito@mp.t.u-tokyo.ac.jp.

Received for review January 12, 2015 and accepted February 24, 2015.

Published online February 24, 2015
10.1021/acsnano.5b00497

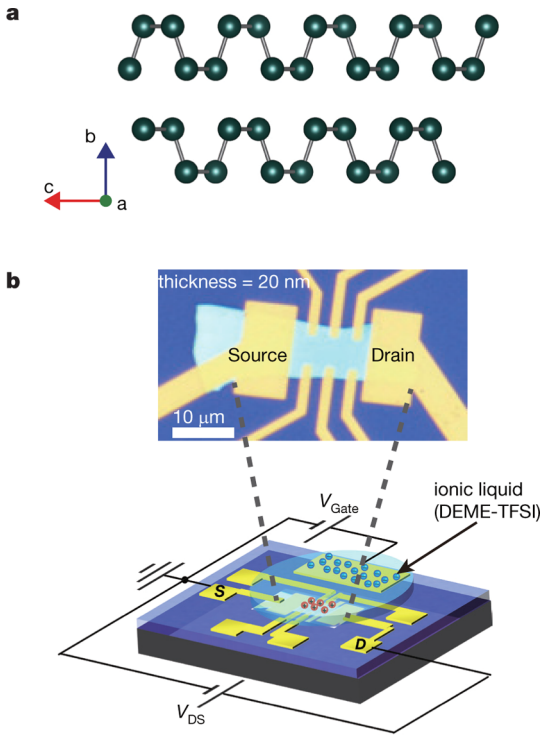

Figure 1. Crystal structure of black phosphorus (BP) and a schematic image of a BP-EDLT. (a) Ball-and-stick model of a BP single crystal. (b) Optical micrograph of a BP thin flake patterned with metal electrodes in a Hall bar configuration (top) and a schematic image of an EDLT device structure (bottom).

functional devices based on BP. For this purpose, an electric-double-layer transistor (EDLT) using ionic liquids as the gate dielectrics is an efficient tool to widely tune the range of the Fermi energy, from the valence to the conduction band.[19−21] The electric-double layer (EDL) formed at liquid/solid interfaces with a ∼1 nm thick Helmholtz layer allows us to effectively accumulate or deplete charge carriers. Therefore, the EDLT offers an opportunity to elucidate the nature of electron transport in BP through the realization of ambipolar transport.

RESULTS AND DISCUSSION

Here, we report on the EDLT operation and electric field control of the ambipolar insulator-to-metal transition in a BP thin flake. We prepared BP thin flakes from a bulk single crystal (Smart-elements, Austria) through a mechanical exfoliation method and transferred the flakes to a SiO_2/Si substrate. We chose the particular flake with a thickness of 20 nm (Figure 1b), as confirmed by atomic force microscopy, as extremely thin flakes (<5 nm) have a low mobility of ∼10 $cm^2/(V\ s)$.[8] We fabricated electrodes (Cr/Au, 5/70 nm) in a Hall bar configuration along with covers (Ti/SiO_2, 5 nm/30 nm) for each electrode, to prevent damaging the Au with the ionic liquid (Figure 1b). Here we did not take the in-plane anisotropy into account because we considered that it did not affect the ambipolar properties.

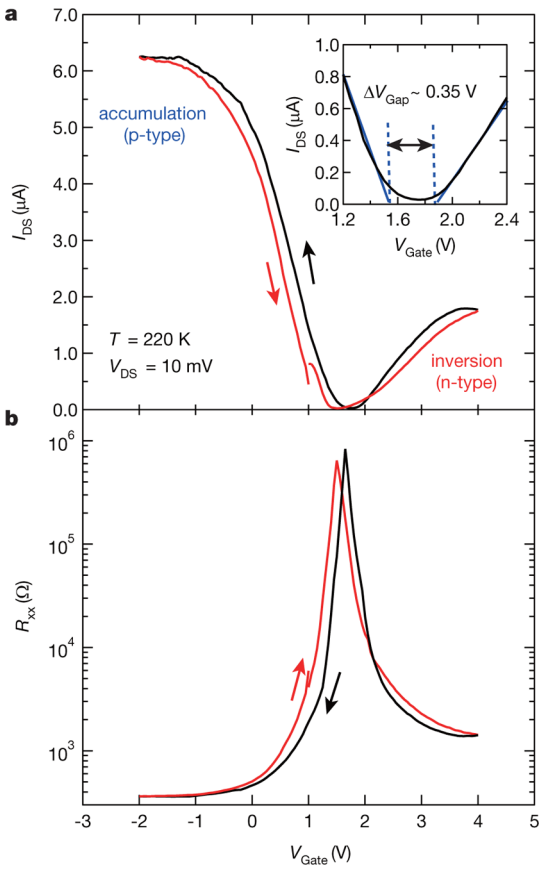

Figure 2. Transfer curve of a BP-EDLT. (a) Source−drain current (I_{DS}) as a function of the gate voltage (V_{Gate}) at V_{DS} = 10 mV, showing an ambipolar operation. The inset shows a magnified image of the threshold voltage. We can extract $\Delta V_{GAP} = V_{TH}^{electron} - V_{TH}^{hole} \cong 0.35$ V by using the V_{Gate}-linear fit represented by the blue solid line. (b) Change in resistance R_{xx} (4-probe) as a function of V_{Gate}.

A droplet of ionic liquid covered both the channel area and the gate electrode. The ionic liquid *N*,*N*-diethyl-*N*-(2-methoxyethyl)-*N*-methylammonium bis(trifluoromethylsulfonyl)imide (DEME-TFSI) was chosen as the gate dielectric.

Figure 2a and b display the ambipolar transfer characteristics of the BP-EDLT after annealing under vacuum at 370 K for 30 min, namely, the source−drain current I_{DS} and 4-probe resistance R_{xx} as a function of the gate voltage V_{Gate} between −2 and 4 V at 220 K with a sweep speed of 10 mV/s. In these measurements, I_{DS} was measured with a fixed source−drain voltage (V_{DS}) of 10 mV and exhibited reversible behavior without any sign of degradation or anomalies due to chemical reactions, in the source−drain current, or in the gate current. Before annealing, the device exhibited only p-type transistor behavior, but, as shown in Figure 2a and b, ambipolar behavior appeared after annealing. This suggests that the influence of adsorbates on BP surfaces, which work as trapping centers for electrons, was partially negated by annealing above room temperature. At V_{Gate} = 0 V, the BP-EDLT is in the normally ON-state with p-type

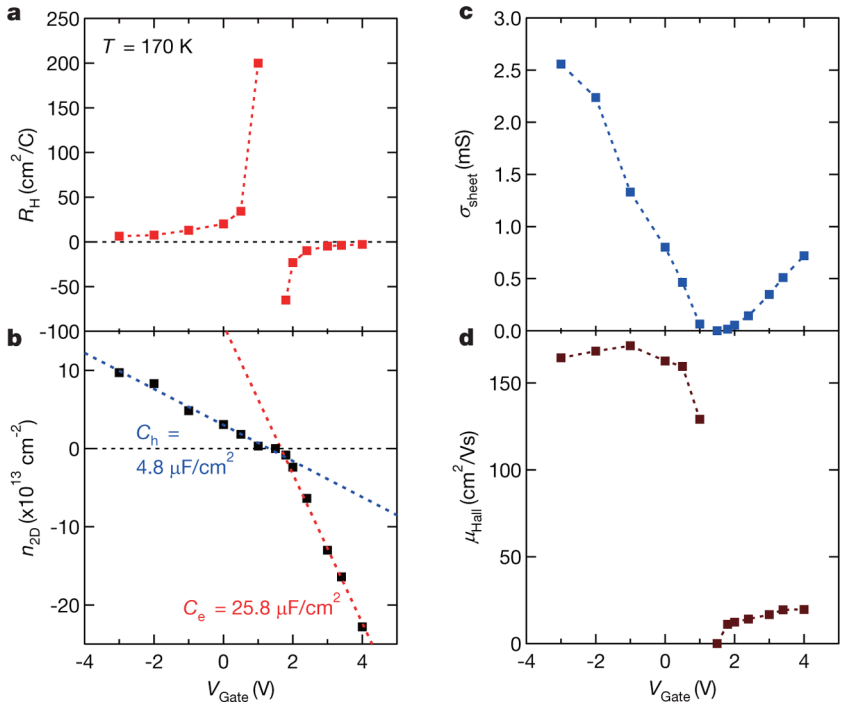

Figure 3. Field-effect modulation of the transport properties of the BP-EDLT. (a) Hall coefficient R_H, (b) sheet carrier density n_{2D}, (c) sheet conductivity σ_{sheet}, and (d) Hall mobility μ_H of the BP-EDLT, as a function of V_{Gate} at 170 K.

behavior, and a negative V_{Gate} therefore accumulates holes. On the other hand, a positive V_{Gate} accumulates electrons while depleting holes, reaching a charge neutrality point in the channel at $V_{Gate} \approx 1.5$ V and forming a sharp R_{xx} peak. A further increase in the positive V_{Gate} generates an electron inversion layer. The minimum OFF current depends on the thickness, as BP flakes are normally p-doped, and in this particular device, the ON−OFF ratio was $\sim 5 \times 10^3$. From the transfer curve shown in Figure 2b, we defined the subthreshold swing $S = ((\mathrm{d} \ln I_{DS})/\mathrm{d}V_G)^{-1}$ at $V_{DS} = 10$ mV with 114 and 118 mV/dec for the electron and hole transport, respectively. These values are much lower than those of SiO_2-based BP-FETs[8] and are slightly higher than the MoS_2 monolayer FET (74 mV/dec).[5] Ambipolar transfer characteristics similar to those observed in our study have also been achieved using solid-gate FETs.[22]

It is known that, for many substances, the band gap can be estimated from the transfer curve in many substances owing to the large capacitance of EDLTs.[23,24] The change in the semiconductor Fermi level position is given by[25]

$$e\Delta V_{Gate} = \Delta E_F + \Delta\phi = \Delta E_F + \frac{e^2 n}{C_G} \qquad (1)$$

where E_F is the material chemical potential and $\Delta\phi$ is the variation in the electrostatic potential, which corresponds to $e^2 n/C_G$ (n is the carrier density and C_G is the geometrical capacitance.). In the case of a normal FET, the second term is usually dominant, as there are localized states in the band gap due to defects in the material, and because the capacitance (C_G) of solid-state gate dielectrics is relatively small. Conversely, EDLTs have a high geometrical capacitance, such that the contribution of the second term in eq 1 can be neglected. Therefore, we can consider that $e\Delta V_{Gate}$ equals ΔE_F for EDLTs. In the present case, the threshold voltages $V_{TH}^{electron}$ and V_{TH}^{hole} were determined to be ~1.88 and ~1.53 V for the electron and hole currents, respectively; the values being extracted from the V_{Gate}-linear fit are shown as a blue solid line (Figure 2a, inset). The difference between the two, $\Delta V_{GAP} = V_{TH}^{electron} - V_{TH}^{hole} \cong 0.35$ V, corresponds to the band gap of the channel material, assuming that the potential drop occurs mainly at the interface between the channel material and the ionic liquid. The obtained value of ≅0.35 eV is roughly consistent with the bulk band gap of ~0.3 V,[26−30] as the thickness of the present BP flake is 20 nm, which is thick enough to be considered a bulk material.

In Figure 3, we summarize the results of the Hall-effect measurements at 170 K, at which the ionic liquid is frozen. The Hall coefficient R_H showed a change in its sign at the charge neutrality point at $V_{Gate} \approx 1.5$ V, confirming the ambipolar behavior of BP. The sheet carrier density, which is directly extracted by using the relation $n_{2D} = 1/eR_H$, is plotted against V_{Gate} in Figure 3b. n_{2D} exhibited a linear behavior showing typical electrostatic charge accumulation. It is noted that the capacitance differs between the two carrier types: 25.8 and 4.8 μF/(V s) for the electron and hole, respectively. While this asymmetric capacitance is quite unexpected, it can still be anticipated when an ionic liquid is used, as the size of the molecular ions

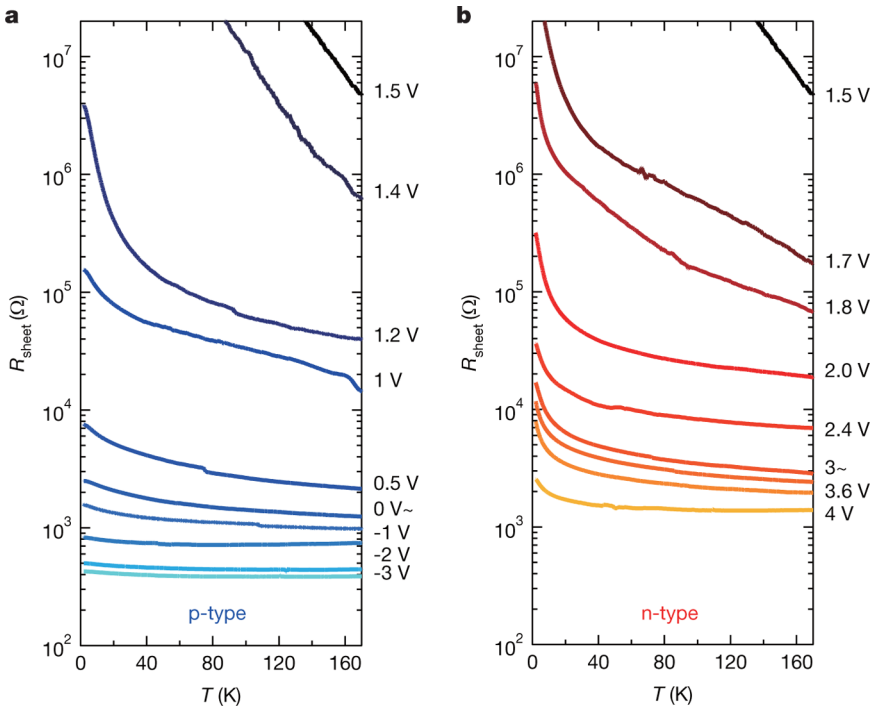

Figure 4. Ambipolar insulator-to-metal transition driven by an electric field. Sheet resistance (R_{sheet}) for (a) hole transport and (b) electron transport as a function of temperature (T), plotted on a semilogarithmic scale, for different gate voltages (V_{Gate}) varying from −3 V to 4 V.

accumulated in the channel differs between positive and negative V_{Gate}. However, the change in the capacitance occurs not at V_{Gate} = 0 V but at the charge neutrality point, $V_{Gate} \approx$ 1.5 V, indicating that the capacitance difference cannot be attributed to the size difference between cations and anions in the ionic liquid. Indeed, a signature of anisotropic capacitance has been observed in BP solid-gated FETs.[8] According to the reported data on gate-dependent R_H, the capacitance C_e and C_h for electron and hole accumulations differs by a factor of 2−5. This is comparable to our results, suggesting that this asymmetric capacitance appears irrespective of the dielectric media (ionic liquid or SiO_2) and could thus be due to the intrinsic properties of BP. Although we do not yet have a clear explanation for this asymmetric behavior, the asymmetric capacitance might suggest a necessity for deeper investigation into the charge accumulation mechanism in EDLTs. In the case of MoS_2, the capacitances for electron and hole channels are approximately symmetric.[31] The difference between BP and MoS_2 is the nominal doping state, which might play a crucial role in the asymmetric capacitance in BP: MoS_2 is insulating (OFF-state), while black phosphorus is heavily hole doped (ON-state).

Figure 3c and d show the sheet conductance σ_{sheet} and the mobility μ_H, respectively, as derived from the Hall-effect measurements. The hole mobility of ~190 $cm^2/(V\ s)$ is much higher than that for electrons at ~20 $cm^2/(V\ s)$. Considering the almost identical effective mass of electrons and holes, a much lower electron mobility exists in the BP-EDLT. This indicates that electron transport is still seriously hindered by shallow trapping centers, which remain after annealing the BP-EDLT in a vacuum at 370 K. Minimizing residual traps is crucial to increasing the electron mobility. It is also noted that the hole mobility is slightly lower than the results of other groups.[8,9] It is well known that the mobility in EDLTs is always lower than in conventional solid gated FETs, as the accumulated carriers themselves work as scattering points. Another cause of the low mobility is the existence of randomly distributed cations on top of the channel, which is another source of carrier scattering. The relatively low mobility reported in the present paper is therefore not an artifact, but is instead an intrinsic effect of the EDLT device. While we believe that there is much room to improve the mobility in EDLTs, we do not believe that air exposure is the dominant cause of the low mobility. This is because the total exposure time to air was less than 1 h, which is small enough to neglect the possibility of sample degradation due to the hydrophilicity. This is especially so considering that a clear change (such as the generation of bubbles) on the surface appears only after exposure to air for 3 days, as has been reported by other groups.[8,32] Potential solutions for this lower mobility are to transfer the black phosphorus thin flake onto a h-BN thin flake or to fabricate a sandwiched structure such as h-BN/BP/h-BN, as reported by other groups.[33−35]

Figure 4a and b show the sheet resistance (R_{sheet}) as a function of the temperature (T) for applied gate

voltages between −3 and 4 V. Despite the 1 order of magnitude lower Hall mobility for the electrons, the accumulated carrier density is larger for the electrons by a factor of more than 2. This results in a significant reduction in resistance by more than 4 orders of magnitude, on both the hole and electron channels. At the same time, we achieved the metallic state, which is defined by the state where $dR/dT > 0$ is realized in the high-temperature regime (above 130 K), although an increase of the resistance due to localization occurred at low temperatures. But we also observed the saturation of the resistance for the hole channel (V_{Gate} = 0, −0.5, −1, −2, and 3 V) and also the electron channel (V_{Gate} = 4 V) at very low temperature. These results are the first observation of ambipolar insulator-to-metal transition in BP using ionic-liquid gating. The continuous tuning of the conductivity and carrier density on the electron side, which has never been reported, will allow us to investigate the electron transport properties as well as the possible ground state of electron-doped BP. Shao *et al*. recently reported on a theoretical prediction that the superconducting state appears in electron-doped phosphorene,[36] a single atomic layer of BP, above $n_{2D} = 1.3 \times 10^{14}$ cm^{-2}, and that a minimum n_{2D} of 2×10^{14} cm^{-2} is necessary for realizing superconductivity above T = 2 K, which is the lowest temperature in our experiment. Unfortunately, we did not observe superconductivity above 2 K. There are several possible reasons for this: one is simply because the electron density was not large enough for attaining superconductivity. Another possibility is that the resistance upturn observed at low temperatures occurred even at the highest gate voltage (Figure 4b), which hinders the occurrence of superconductivity. The third possibility is that superconductivity might be restricted only in monolayer BP. Further improvement in EDLT performance may be required to achieve electric-field-induced superconductivity.

To have further insight into the resistance upturn at low temperature, we plot the zoom-in temperature-dependent conductivity below 20 K for hole and electron accumulations in Figure 5a and b, respectively. These figures showed contrasting behavior of hole and electron accumulation regions, namely, that the temperature dependence for the electron accumulation is steeper than that for the hole accumulations. To understand this contrasting behavior, we analyzed its temperature dependence taking into account the quantum correction in terms of the weal localization (WL) model, which assumes not only elastic scattering but also inelastic scattering of charge carriers. This model predicts distinctive dimensionality dependence: In the case of 2D systems, the contribution of WL is approximated by

$$\Delta\sigma_{2D} = \frac{ape^2}{2\hbar} \ln T \qquad (2)$$

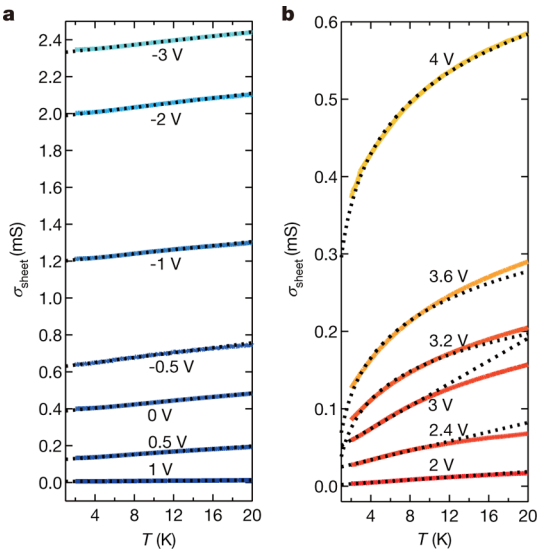

Figure 5. Temperature dependence of the sheet conductance (σ_{sheet}) for (a) hole transport and (b) electron transport as a function of temperature (T) for different gate voltages (V_{Gate}). The dashed lines show the 2D-WL model, and the dashed curved lines show the 3D-WL model.

where a and p are the constant values, e is the elementary charge, and $\hbar$ is the Plank constant divided by 2π. In the 3D case, it is described by

$$\Delta\sigma_{3D} = \frac{ce^2}{\hbar}\sqrt{\frac{\Gamma}{D}}T^{p/2} \qquad (3)$$

where c and Γ are constant values and D is the diffusion coefficient. If the scattering is due to the electron−phonon scattering, p = 2 (T-linear) shows the normal Fermi liquid and $p < 2$ shows the disordered system. As shown in Figure 5a, the temperature-dependent conductance for the hole accumulation is almost linear and is well fitted by the 3D model of eq 3. On the other hand, for the electron-accumulated region, the steeper temperature dependence is well fitted by the 2D model of eq 2. However, just above the charge neutrality point at 3 and 2.4 V, the $\sigma_{sheet}(T)$ values deviate from the 2D-WL fitting line and are closer to the T-linear line, or the expression of the 3D-WL model (p = 2).

The above observations led us to propose the following scenario of ambipolar charge accumulation associated with the dimensionality change from 2D to 3D nature. First, at very positive high gate voltages, where the inversion layer of electrons is formed, the quantum confinement of electrons is very strong, the electrons are confined in a very narrow region (∼1 nm), and the other region of the whole flake is depleted, resulting in 2D WL behavior. With decreasing gate voltage, the thickness of the accumulation layer is larger with reduced electron density, driving a 2D−3D crossover of WL for the electron channel. At the charge neutrality point V_G = 1.5 V, both electron and hole carriers are completely depleted. When V_G is

further reduced, hole doping starts, and at $V_G = 0$ V, the whole BP flake returns back to the uniformly hole-doped state and the hole carriers behave as 3D. The enhancement of hole conductivity at $V_G = -3$ V over $V_G = 0$ V is only 6 times at 2 K, indicating that the bulk flake is still making a considerable contribution to the observed hole conductivity, resulting in the more 3D-like WL behavior for the hole side. The above scenario is consistent with the difference in mobility of electrons and holes shown in Figure 3d. Since the electron carriers are strongly confined at the surface of BP, they are more subjected to surface disorder than hole carriers because the contribution from the bulk carriers is not negligible even in the hole accumulation region. This may be another case of the significantly lower mobility of electrons in addition to the shallow trapping centers discussed above. In the case of TMDCs, we observed WL, but we did not observe the 2D−3D crossover of localization. The situation in TMDC is different from that in BP, particularly in the present case, because BP is a nominally hole-doped system. The carrier density is $\sim 3 \times 10^{13}$ cm^{-2} at 0 V, which is only one-third of the maximum carrier density of hole channels, whereas TMDC is nominally in the OFF-state. This means that the bulk carrier in the of BP flake is still making a considerable contribution to the observed hole conductivity, while carriers accumulated only at the surface of TMDCs behave like 2D.

CONCLUSION

In conclusion, we have presented a comprehensive view of the ambipolar transistor operation on a BP thin flake with an EDLT configuration. The band gap was determined as ≅0.35 V, which is consistent with that of the bulk material. Hall-effect measurements revealed asymmetric capacitances and differences in mobility between electrons and holes. In addition, we succeeded in inducing ultrahigh carrier density and in tuning BP from a typical insulating state to a metallic state in both carrier types. Also, examination of the temperature dependence of resistance at low temperature revealed a 2D−3D crossover when V_G is scanned from electrons to holes. The 3D-like localization behavior is ascribed to the contribution from the hole carriers that are unintentionally doped over the whole flake. These results suggest a necessity of fabrication of undoped BP flake for the observed intrinsic 2D behavior of gate-induced carriers. The present work provides useful information for fabrication of BP-based electronics devices for the fabrication of functional devices, such as lateral p−n junctions and tunnel diodes, due to the intrinsic narrow band gap.

METHODS

Device Fabrication. Black phosphorus thin flakes obtained from Smart-elements (http://www.smart-elements.com/) were mechanically exfoliated and transferred onto 300 nm thick SiO_2 layers on highly doped Si substrates. Since black phosphorus thin flakes are highly unstable in air, immediately after the exfoliation, we covered a resist (ZEP 520 A). The ZEP was coated onto the SiO_2/Si substrate by using a programmable spin-coater. Two-step spinning was performed: 500 rpm for the initial 3 s after ZEP dropping, followed by 4000 rpm for the subsequent 50 s. The coated substrate was heated for 3 min on a covered hot-plate at 423 K. Next electron-beam lithography was used to pattern the source/drain contact electrodes (see main text). We removed the resist that remained on the substrate by immersing the substrate in *N*-methyl-2-pyrrolidone for 40−60 min at 323 K, then spraying acetone and immersing in isopropyl alcohol.

Transport Measurements. All the transport measurements were performed in a Physical Property Measurement System (PPMS, Quantum Design, Inc.) in a 2−300 K temperature range up to 9 T under He-purged conditions. In the cooling effect measurement, when we cooled and warmed with a sweeping rate of 1 K/min, we maintained the rate in the whole temperature scan. In the measurement of the gating effect, we first cooled from 300 K to 220 K without gating, applied the gate voltage at 220 K, cooled and warmed between 220 and 2 K, and released the gate voltage at 240 K. The entire gating experiment was performed with a scanning rate of 1 K/min.

Conflict of Interest: The authors declare no competing financial interest.

Acknowledgment. This work was supported by the Strategic International Collaborative Research Program (SICORP-LEMSUPER) of the Japan Science and Technology Agency, Grant-in-Aid for Specially Promoted Research (No. 25000003) from JSPS.

REFERENCES AND NOTES

1. Novoselov, K. S.; Geim, A. K.; Morozov, S. V.; Jiang, D.; Zhang, Y.; Dubonos, S. V.; Grigorieva, I. V.; Firsov, A. A. Electric Field Effect in Atomically Thin Carbon Films. *Science* **2004**, *306*, 666–669.
2. Novoselov, K. S.; Geim, A. K.; Morozov, S. V.; Jiang, D.; Katsnelson, M. I.; Grigorieva, I. V.; Dubonos, S. V.; Firsov, A. A. Two-Dimensional Gas of Massless Dirac Fermions in Graphene. *Nature* **2005**, *438*, 197–200.
3. Zhang, Y.; Tan, Y.-W.; Stormer, H. L.; Kim, P. Experimental Observation of the Quantum Hall Effect and Berry's Phase in Graphene. *Nature* **2005**, *438*, 201–204.
4. Novoselov, K. S.; Jiang, D.; Schedin, F.; Booth, T. J.; Khotkevich, V. V.; Morozov, S. V.; Geim, A. K. Two-Dimensional Atomic Crystals. *Proc. Natl. Acad. Sci. U.S.A.* **2005**, *102*, 10451–10453.
5. Radisavljevic, B.; Radenovic, A.; Brivio, J.; Giacometti, V.; Kis, A. Single-Layer MoS_2 Transistors. *Nat. Nanotechnol.* **2011**, *6*, 147–150.
6. Zhang, Y. J.; Oka, T.; Suzuki, R.; Ye, J. T.; Iwasa, Y. Electrically Switchable Chiral Light-Emitting Transistor. *Science* **2014**, *344*, 725–728.
7. Mak, K. F.; McGill, K. L.; Park, J.; McEuen, P. L. The Valley Hall Effect in MoS_2 Transistors. *Science* **2014**, *344*, 1489–1492.
8. Li, L.; Yu, Y.; Ye, G. J.; Ge, Q.; Ou, X.; Wu, H.; Feng, D.; Chen, X. H.; Zhang, Y. Black Phosphorus Field-Effect Transistors. *Nat. Nanotechnol.* **2014**, *9*, 372–377.
9. Liu, H.; Neal, A. T.; Zhu, Z.; Luo, Z.; Xu, X.; Tománek, D.; Ye, P. D. Phosphorene: An Unexplored 2D Semiconductor with a High Hole Mobility. *ACS Nano* **2014**, *8*, 4033–4041.
10. Qiao, J.; Kong, X.; Hu, Z.-X.; Yang, F.; Ji, W. High-Mobility Transport Anisotropy and Linear Dichroism in Few-Layer Black Phosphorus. *Nat. Commun.* **2014**, *5*, 4475.
11. Xia, F.; Wang, H.; Jia, Y. Rediscovering Black Phosphorus as an Anisotropic Layered Material for Optoelectronics and Electronics. *Nat. Commun.* **2014**, *5*, 4458.

12. Slater, J. C.; Koster, G. F.; Wood, J. H. Symmetry and Free Electron Properties of the Gallium Energy Bands. *Phys. Rev.* **1962**, *302*, 1307–1317.
13. Brown, A.; Rundqvist, S. Refinement of the Crystal Structure of Black Phosphorus. *Acta Crystallogr.* **1965**, *19*, 684–685.
14. Cartz, L.; Srinivasa, S. R.; Riedner, R. J.; Jorgensen, J. D.; Worlton, T. G. Effect of Pressure on Bonding in Black Phosphorus. *J. Chem. Phys.* **1979**, *71*, 1718.
15. Jamieson, J. Crystal Structures Adopted by Black Phosphorus at High Pressures. *Science* **1963**, *29*, 1291–1292.
16. Vanderborgh, C.; Schiferl, D. Raman Studies of Black Phosphorus from 0.25 to 7.7 GPa at 15 K. *Phys. Rev. B* **1989**, *40*, 9595–9599.
17. Wittig, J.; Matthias, B. Superconducting Phosphorus. *Science* **1968**, *160*, 994–995.
18. Kawamura, H.; Shirotani, I.; Tachikawa, K. Anomalous Superconductivity in Black Phosphorus under High Pressures. *Solid State Commun.* **1984**, *10*, 879–881.
19. Efetov, D. K.; Kim, P. Controlling Electron-Phonon Interactions in Graphene at Ultrahigh Carrier Densities. *Phys. Rev. Lett.* **2010**, *105*, 256805.
20. Ye, J. T.; Zhang, Y. J.; Akashi, R.; Bahramy, M. S.; Arita, R.; Iwasa, Y. Superconducting Dome in a Gate-Tuned Band Insulator. *Science* **2012**, *338*, 1193–1196.
21. Shimotani, H.; Asanuma, H.; Tsukazaki, A.; Ohtomo, A.; Kawasaki, M.; Iwasa, Y. Insulator-to-Metal Transition in ZnO by Electric Double Layer Gating. *Appl. Phys. Lett.* **2007**, *91*, 082106.
22. Das, S.; Demarteau, M.; Roelofs, A. Ambipolar Phosphorene Field Effect Transistor. *ACS Nano* **2014**, 11730–11738.
23. Braga, D.; Gutiérrez Lezama, I.; Berger, H.; Morpurgo, A. F. Quantitative Determination of the Band Gap of WS_2 with Ambipolar Ionic Liquid-Gated Transistors. *Nano Lett.* **2012**, *12*, 5218–5223.
24. Yomogida, Y.; Pu, J.; Shimotani, H.; Ono, S.; Hotta, S.; Iwasa, Y.; Takenobu, T. Ambipolar Organic Single-Crystal Transistors Based on Ion Gels. *Adv. Mater.* **2012**, *24*, 4392–4397.
25. Ye, J. T.; Craciun, M.; Koshinod, M.; Russoe, S.; Inoue, S.; Yuan, H.; Shimotania, H.; Morpurgo, A. F.; Iwasa, Y. Accessing the Transport Properties of Graphene and Its Multilayers at High Carrier Density. *Proc. Natl. Acad. Sci. U.S.A.* **2011**, *108*, 13002–13006.
26. Warschauer, D. Electrical and Optical Properties of Crystalline Black Phosphorus. *J. Appl. Phys.* **1963**, *34*, 1853–1860.
27. Akahama, Y.; Endo, S.; Narita, S. Electrical Properties of Black Phosphorus Single Crystals. *J. Phys. Soc. Jpn.* **1983**, *52*, 2148–2155.
28. Keyes, R. The Electrical Properties of Black Phosphorus. *Phys. Rev.* **1953**, *92*, 580–584.
29. Maruyama, Y.; Suzuki, S.; Kobayashi, K.; Tanuma, S. Synthesis and Some Properties of Black Phosphorus Single Crystals. *Phys. B+C* **1981**, 99–102.
30. Rodin, A. S.; Carvalho, A.; Castro Neto, A. H. Strain-Induced Gap Modification in Black Phosphorus. *Phys. Rev. Lett.* **2014**, *112*, 176801–176805.
31. Zhang, Y.; Ye, J.; Matsuhashi, Y.; Iwasa, Y. Ambipolar MoS_2 Thin Flake Transistors. *Nano Lett.* **2012**, *12*, 1136–1140.
32. Castellanos-Gomez, A.; Vicarelli, L.; Prada, E.; Island, J. O.; Narasimha-Acharya, K. L.; Blanter, S. I.; Groenendijk, D. J.; Buscema, M.; Steele, G. A.; Alvarez, J. V. Isolation and Characterization of Few-Layer Black Phosphorus. *2D Mater.* **2014**, *1*, 025001.
33. Li, L.; Ye, G. J.; Tran, V.; Fei, R.; Chen, G.; Wang, H.; Wang, J.; Watanabe, K.; Taniguchi, T.; Yang, L. Quantum Oscillations in Black Phosphorus Two-Dimensional Electron Gas. arXiv:1411.6572, **2014**.
34. Gillgren, N. *et al.* Gate Tunable Quantum Oscillations in Air-Stable and High Mobility Few-Layer Phosphorene Heterostructures. arXiv:1412.0717, **2014**.
35. Chen, X.; Wu, Y.; Wu, Z.; Xu, S.; Wang, L.; Han, Y.; Han, T.; He, Y.; Cai, Y.; Wang, N. High Quality Sandwiched Black Phosphorus Heterostructure and Its Quantum Oscillations. arXiv:1412.1357, **2014**.
36. Shao, D. F.; Lu, W. J.; Lv, H. Y.; Sun, Y. P. Electron-Doped Phosphorene: A Potential Monolayer Superconductor. arXiv:1405.0092, **2014**.